JOURNAL OF GUIDANCE, CONTROL, AND DYNAMICS
Vol. 44, No. 2, February 2021

Engineering Notes

CubeSat Adaptive Attitude Control with Uncertain Drag Coefficient and Atmospheric Density

Runhan Sun,* Camilo Riano-Rios,† Riccardo Bevilacqua,‡
Norman G. Fitz-Coy,§ and Warren E. Dixon¶
University of Florida, Gainesville, Florida 32603

https://doi.org/10.2514/1.G005515

I. Introduction

A. Motivation and Literature Review

CUBESATS are small spacecraft typically used in low Earth orbit (LEO). At LEO, spacecraft interact with low-density atmosphere and experience atmospheric drag. Atmospheric drag is commonly considered as a perturbation in the equations of motion for an orbiting spacecraft, but it can also be exploited to maneuver the spacecraft using a drag maneuvering device (DMD) (e.g., [1,2]).

Previous work in [3,4] investigated orbital maneuvering, collision avoidance, and attitude stabilization by a DMD-equipped CubeSat. However, these algorithms assume that all drag surfaces (DSs) are evenly deployed at all times. In real operation, lengths of DSs are hard to deploy equally due to manufacturing tolerances, potentially resulting in unbalanced torques with respect to the center of mass of the spacecraft because the DSs are controlled independently.

CubeSat missions usually require maintaining attitude for communication or sensing purposes. Atmospheric torque and magnetic torque are used to maintain the attitude of a CubeSat for sensing tasks in [5], where a DMD-like distribution of fixed DSs is used to improve the performance of magnetic-based attitude control. Roto-translational control using atmospheric drag has also been investigated in [6,7], where a switching strategy for on-off virtual thrusters and a sliding mode controller are developed via a Lyapunov-based method.

The atmospheric and gravity gradient torques imposed on a spacecraft heavily depend on its geometry. The distribution and degrees of freedom of the DSs directly influence the capability of the spacecraft to control or stabilize its attitude. Common designs have two degrees of freedom for each DS, e.g., extend/retract and rotation about an axis, which results in an undesirable increase in complexity and uncertainty. The hardware specifications of the DMD considered in this paper are stated in [2].

Received 6 July 2020; revision received 28 August 2020; accepted for publication 17 November 2020; published online 24 December 2020.

*Graduate Student, Department of Mechanical and Aerospace Engineering; runhansun@ufl.edu.
†Graduate Student, Department of Mechanical and Aerospace Engineering; crianorios@ufl.edu.
‡Associate Professor, Department of Mechanical and Aerospace Engineering; bevilr@ufl.edu. Associate Fellow AIAA.
§Associate Professor, Department of Mechanical and Aerospace Engineering; nfc@ufl.edu. Associate Fellow AIAA.
¶Ebaugh Professor, Department of Mechanical and Aerospace Engineering; wdixon@ufl.edu.

Atmospheric torque in CubeSat attitude controllers often assumes that the drag coefficient of the spacecraft and atmospheric density are known or can be determined. For example, the drag coefficient for the spacecraft is estimated based on its shape in [8]. For atmospheric density estimation, Ref. [9] can be used to calculate the density at various altitudes to characterize the behavior of the satellite under average orbital conditions. For a specific orbit, more accurate density models such as the NRLMSISE-00 model [10] can be used for estimation. Although there are several models for atmospheric density, solar and geomagnetic activities produce changes that are difficult to model and predict.

The gravity gradient torque experienced by a spacecraft due to the gradient of gravitational forces along its body is exploited for attitude stabilization in [11]. Oscillations about the three body axes propagated from the initial conditions were observed, and improved performance was obtained by deploying DSs along the pitch axis. Gravity gradient and aerodynamic torques were also used in [12] for attitude control of CubeSat using reaction wheels and applying constraints on the actuator torque. Recently, techniques for attitude stabilization using the DMD have been proposed by combining gravity gradient torque with magnetic and aerodynamic torques in [13,14], respectively.

Adaptive control methods can be used to compensate for uncertainties in the system model. However, the parameter estimates may not converge to the true values without persistent excitation (PE) [15–17]. In general, the PE condition cannot be guaranteed a priori for nonlinear systems and cannot be verified online. Specifically, the PE condition requires the system to be persistently excited over the infinite time integral. Motivated by the desire to learn the true parameters while relaxing the PE requirement, an adaptive update scheme known as concurrent learning (CL) was developed in [18,19] assuming that higher order states could be measured and filtered. The finite excitation (FE) condition used in CL requires the system to be sufficiently excited over a finite time period, and CL updates estimates of the constant unknown parameters based on input and output data of the dynamic system. The FE condition is a verifiable condition that can be checked online by examining the eigenvalue of a matrix constructed of input–output data collected concurrent to the control execution. More recent developments eliminate the need for higher-order state measurements through integral concurrent learning (ICL) [20–22].

B. Design Challenges

In this paper, an adaptive controller is designed to track the desired attitude trajectory of the spacecraft in [2] with a DMD that provides one degree of freedom for each of its four DSs. Each DS is offset by 90 deg with a fixed inclination angle of 20 deg with respect to the anti-ram surface of the spacecraft as depicted in Fig. 1. In Fig. 1, the spacecraft's body-fixed frame is attached to the center of mass of the spacecraft, with the $\hat{b}_1$ axis aligned with the ram direction, the $\hat{b}_2$ axis on the nadir facing side of the spacecraft, and the $\hat{b}_3$ axis selected to complete the dextral orthogonal coordinate system. The DSs are aligned such that surfaces DS1 and DS3 are deployed in the $\hat{b}_1\hat{b}_3$ plane, and surfaces DS2 and DS4 deployed in the $\hat{b}_1\hat{b}_2$ plane. The centroidal inertia tensor of the spacecraft is dependent on the deployed length of each surface. Also shown in Fig. 1 is an orbiting coordinate frame attached to the center of mass of the spacecraft. The $\hat{o}_2$ axis is aligned with the orbit's angular momentum vector, the $\hat{o}_3$ axis points in the zenith direction, and the $\hat{o}_1$ axis completes the dextral orthogonal triad.

The control objective is to track a given desired attitude trajectory using the atmospheric and gravity gradient torques produced by modulating the length and velocity of the DMD DSs while identifying uncertain parameters associated with the drag coefficient and

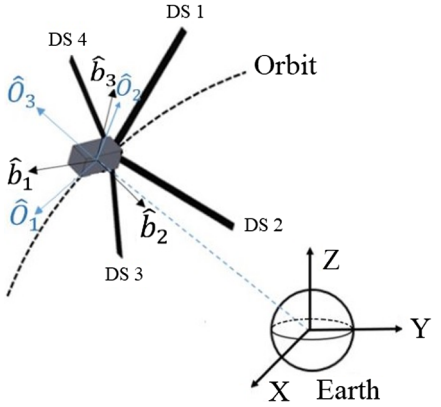

Fig. 1 Inertial, orbit, and body coordinate systems.

atmospheric density. The atmospheric and gravity gradient torques are included in the nonlinear dynamic model without the typical small angle assumption. Moreover, the control inputs are coupled with the time-varying inertia tensor due to the changing lengths of the DSs of the DMD. Specifically, because attitude tracking is achieved through modulating the DMD, the torques resulting from the time derivative of the inertia tensor term are included in the subsequent analysis, generalizing typical results such as [6,7,14]. Given the time derivative of the inertia tensor, the control inputs include both lengths and velocities of DSs instead of only the lengths. To track the desired attitude trajectory, the control inputs need to satisfy the subsequently designed auxiliary control using an optimization algorithm to adjust the configuration of the surfaces. The development is further complicated by the fact that a drag coefficient and the atmospheric density are multiplicative uncertainties with the control input. Lyapunov-based techniques are used to guide the design of an ICL controller that simultaneously identifies the uncertain parameters without requiring the traditional PE condition. Instead, the verifiable FE condition (subsequently described in Sec. VI.B) is used. Specifically, before the FE condition is satisfied, a Lyapunov-based analysis is used to prove that the tracking errors are bounded. Once the FE condition is satisfied, further analysis is used to conclude uniformly ultimately bounded parameter identification. Two simulation examples are provided to demonstrate the performance of the proposed approach. The developed controller was able to track a desired trajectory with less than $\pm 8.0 \times 10^{-2}$ deg steady-state error in Euler angle representation, while simultaneously identifying the uncertain drag coefficient and atmospheric density with up to 0.93% error.

II. Preliminaries

Let $\mathbb{R}$ and $\mathbb{Z}$ denote the set of real numbers and integers, respectively, where $\mathbb{R}_{\geq 0} \triangleq [0, \infty)$, $\mathbb{R}_{>0} \triangleq (0, \infty)$, $\mathbb{Z}_{\geq 0} \triangleq \mathbb{R}_{\geq 0} \cap \mathbb{Z}$, and $\mathbb{Z}_{>0} \triangleq \mathbb{R}_{>0} \cap \mathbb{Z}$. Let $p \in \mathbb{Z}_{>0}$. The $p \times p$ identity matrix is denoted by I_p. The skew symmetric matrix $a^{\times} \in \mathbb{R}^{3\times 3}$ for a vector $a \triangleq [\, a_1 \quad a_2 \quad a_3 \,]^T \in \mathbb{R}^3$ is defined as

$$a^{\times} \triangleq \begin{bmatrix} 0 & -a_3 & a_2 \\ a_3 & 0 & -a_1 \\ -a_2 & a_1 & 0 \end{bmatrix}$$

The cross-product operator is denoted as $\times$. Note that the vector cross product can be expressed as the product of a skew symmetric matrix and a vector (i.e., $b \triangleq [\, b_1 \quad b_2 \quad b_3 \,]^T \in \mathbb{R}^3$), e.g., $a \times b = a^{\times} b$. The Euclidean norm of a vector $m \in \mathbb{R}^p$ is denoted by $\|m\| \triangleq \sqrt{m^T m}$, and the absolute value of a scalar $n \in \mathbb{R}$ is denoted by $|n|$. The notations $\lambda_{\min}\{\cdot\}$ and $\lambda_{\max}\{\cdot\}$ denote the minimum and maximum eigenvalues of $\{\cdot\}$, respectively.

III. Attitude Dynamics

The symmetric centroidal moment of inertia tensor about the center of mass of the spacecraft is denoted as $J \in \mathbb{R}^{3\times 3}$ in the body coordinate system.[**] The angular velocity of the spacecraft with respect to the inertial reference frame can be defined as $\omega \in \mathbb{R}^3$ in the body coordinate system. The atmospheric torque $\tau_{AT} \in \mathbb{R}^3$ can be obtained as [14]

$$\tau_{AT} = \sum_{j=1}^{4} r_j^{\times} F_{d,j}, \quad j = 1, 2, 3, 4 \tag{1}$$

where $r_j \in \mathbb{R}^3$ denotes the vector points from the center of mass of the spacecraft to the geometric center of the jth DS expressed in the body coordinate system, and $F_{d,j} \in \mathbb{R}^3$ denotes the drag force generated by the jth DS of the DMD. The drag force $F_{d,j} \in \mathbb{R}^3$ can be expressed as [14]

$$F_{d,j} = -\frac{1}{2} C_D \rho L_j w_b \|v_{\perp,j}\|^2 v_r \tag{2}$$

where $C_D \in \mathbb{R}_{>0}$ denotes the uncertain drag coefficient of the DS (assumed equal for all DSs), $\rho \in \mathbb{R}_{>0}$ is a constant uncertain atmospheric density,[††] $w_b \in \mathbb{R}_{>0}$ is the width of the DS, $L_j \in \mathbb{R}_{\geq 0}$ and $v_{\perp,j} \in \mathbb{R}$ denote the length and the component of the spacecraft's velocity with respect to the atmosphere that is perpendicular to the jth DS, respectively, and $v_r \in \mathbb{R}^3$ denotes the unit vector in the direction of the velocity vector of the spacecraft with respect to the atmosphere expressed in the body coordinate system. The gravity gradient torque $\tau_{GG} \in \mathbb{R}^3$ can be obtained as

$$\tau_{GG} = \frac{3GM_{\oplus}}{\|R_c\|^5} R_c^{\times} J R_c \tag{3}$$

where $G \in \mathbb{R}_{>0}$ denotes the universal gravitational constant, $M_{\oplus} \in \mathbb{R}_{>0}$ denotes the mass of the Earth, and $R_c \in \mathbb{R}^3$ denotes the vector that goes from the center of the Earth to the center of mass of the spacecraft.[‡‡] Based on Eqs. (1–3), the spacecraft attitude dynamics are

$$\dot{J}\omega + J\dot{\omega} + \omega^{\times} J\omega = \tau_{AT} + \tau_{GG} \tag{4}$$

Remark 1: Considering that the material of the DMD surfaces is Austenitic 316 stainless steel [2], it is assumed that these surfaces do not contribute on the magnetic disturbance torques of the CubeSat. Moreover, the design of the spacecraft does not include permanent magnets or high magnetic hysteresis materials. The magnitude of the residual magnetic moment of the spacecraft, and the associated maximum magnetic disturbance torque have been computed following the guidelines in [23] for a class II spacecraft and the procedure described in [24]. The resulting maximum magnetic disturbance torque is 3.95×10^{-7} N · m, which is considered negligible for the purpose of this work given the control authority in the order of 10^{-4} N · m that results from the ability of significantly extending/retracting the surfaces and their influence on the inertia matrix of the spacecraft.

IV. Control Design

A. Control Objective

The control objective is to track a given desired spacecraft attitude trajectory using the atmospheric and gravity gradient torques produced by controlling the length and velocity of the DSs of a DMD

[**] Unless otherwise specified, time dependence is suppressed in equations and definitions.

[††] For illustration purpose, the atmospheric density is assumed to be a constant instead of a time-varying function [1,5].

[‡‡] The norm of the vector R_c can be upper bounded by a positive constant, which means that the distance that goes from the center of the Earth to the center of mass of the spacecraft is finite.

device. The atmospheric torque in Eq. (1) and the gravity gradient torque in Eq. (3) depend on the spacecraft's configuration and lengths of DSs.

An impediment to develop a controller for Eq. (4) is that the subsequently designed auxiliary control inputs are multiplied by an uncertain drag coefficient C_D and an uncertain atmospheric density ρ. Moreover, the inertia of the spacecraft is changing with the length of DSs, and DSs affect the amount of atmospheric torque that can be generated. Yet, the atmospheric torque is a function of parametric uncertainties (i.e., C_D and ρ). The system dynamics can be expressed as a product of a nonlinear regression matrix and a vector of uncertain constants. Based on this parameterization, an ICL adaptive update law is designed to yield a uniformly ultimately bounded result of a given attitude trajectory and parameter estimation provided that a finite-time sufficient excitation condition is satisfied.

To facilitate the subsequent control development, the unit quaternion $q(q_0, q_v) \in \mathbb{R}^4$ with $q_0 \in \mathbb{R}$ and $q_v \in \mathbb{R}^3$ [25] is used to describe the orientation of the spacecraft with respect to the inertial reference frame expressed in the body coordinate system, with the property

$$q_v^T q_v + q_0^2 = 1 \tag{5}$$

The rotational kinematics of the rigid-body spacecraft can be determined as

$$\dot{q}_v = \frac{1}{2}(q_v^\times + q_0 I_3)\omega \tag{6}$$

$$\dot{q}_0 = -\frac{1}{2} q_v^T \omega \tag{7}$$

The rotation matrices that bring the inertial reference frame onto body frame $R \in \mathbb{R}^{3\times3}$ and the inertial reference frame onto the desired body frame $R_d \in \mathbb{R}^{3\times3}$ are defined as

$$R \triangleq \left(q_0^2 - q_v^T q_v\right) I_3 + 2 q_v q_v^T - 2 q_0 q_v^\times \tag{8}$$

$$R_d \triangleq \left(q_{0d}^2 - q_{vd}^T q_{vd}\right) I_3 + 2 q_{vd} q_{vd}^T - 2 q_{0d} q_{vd}^\times \tag{9}$$

respectively, where $q_d(q_{0d}, q_{vd}) \in \mathbb{R}^4$, with $q_{0d} \in \mathbb{R}$ and $q_{vd} \in \mathbb{R}^3$ describing the desired orientation of the spacecraft with respect to the inertial reference frame expressed in the desired body coordinate system. Using Eqs. (6) and (7), ω can be expressed in terms of the quaternion as

$$\omega = 2\left(q_0 \dot{q}_v - q_v \dot{q}_0\right) - 2 q_v^\times \dot{q}_v \tag{10}$$

Similarly, the desired angular velocity of the spacecraft with respect to the inertial reference frame is expressed in the desired body coordinate system as

$$\omega_d = 2(q_{0d}\dot{q}_{vd} - q_{vd}\dot{q}_{0d}) - 2 q_{vd}^\times \dot{q}_{vd} \tag{11}$$

The components $e_v \in \mathbb{R}^3$ and $e_0 \in \mathbb{R}$ of the quaternion tracking error $e(e_0, e_v) \in \mathbb{R}^4$ are defined as

$$e_v \triangleq q_{0d} q_v - q_0 q_{vd} + q_v^\times q_{vd} \tag{12}$$

$$e_0 \triangleq q_0 q_{0d} + q_v^T q_{vd} \tag{13}$$

respectively. From the definitions of the quaternion tracking errors in Eqs. (12) and (13), the following constraint holds [26]:

$$e_v^T e_v + e_0^2 = 1 \tag{14}$$

where

$$0 \le \|e_v\| \le 1$$
$$0 \le |e_0| \le 1$$

To quantify the objective, the rotation matrix that brings the desired body frame onto body frame denote by $\tilde{R}(e_0, e_v) \in \mathbb{R}^{3\times3}$ is defined as

$$\tilde{R} \triangleq R R_d^T \tag{15}$$

Substituting Eqs. (8), (9), (12), and (13) into Eq. (15) yields

$$\tilde{R} = \left(e_0^2 - e_v^T e_v\right) I_3 + 2 e_v e_v^T - 2 e_0 e_v^\times \tag{16}$$

The attitude tracking control objective is

$$\tilde{R} \to I_3 \text{ as } t \to \infty \tag{17}$$

Based on Eqs. (12–14) and Eq. (16), the attitude tracking objective in Eq. (17) is achieved if [26]

$$\|e_v\| \to 0 \Rightarrow |e_0| \to 1 \tag{18}$$

B. Control Development

To facilitate the control development, the angular velocity of the spacecraft with respect to the desired body coordinate system expressed in body coordinate system, denoted by $\tilde{\omega} \in \mathbb{R}^3$, is defined as

$$\tilde{\omega} \triangleq \omega - \tilde{R}\omega_d \tag{19}$$

An auxiliary signal $r \in \mathbb{R}^3$ is defined as

$$r \triangleq \dot{e}_v + \alpha e_v \tag{20}$$

where $\alpha \in \mathbb{R}^{3\times3}_{>0}$ is a constant, positive-definite, diagonal, control gain matrix. The time derivative of the quaternion tracking error in Eqs. (12) and (13) can be written as [27]

$$\dot{e}_v = \frac{1}{2}(e_v^\times + e_0 I_3)\tilde{\omega} \tag{21}$$

and

$$\dot{e}_0 = -\frac{1}{2} e_v^T \tilde{\omega} \tag{22}$$

respectively. Taking the time derivative of Eq. (20) yields

$$\dot{r} = Y\Theta + \alpha \dot{e}_v \tag{23}$$

where

$$Y\Theta = \frac{1}{2}(\dot{e}_v^\times + \dot{e}_0 I_3)\tilde{\omega} + \frac{1}{2}(e_v^\times + e_0 I_3)\Big(J^{-1}\tau_{AT} + J^{-1}\tau_{GG} - J^{-1}\dot{J}\omega - J^{-1}\omega^\times J\omega + \tilde{\omega}^\times \widetilde{R}\omega_d - \widetilde{R}\dot{\omega}_d\Big) \tag{24}$$

with the fact that

$$\dot{\widetilde{R}} = -\tilde{\omega}^\times \widetilde{R}$$

In Eq. (24), the measurable nonlinear regression matrix $Y \in \mathbb{R}^{3\times2}$ can be expressed in terms of the inertia tensor, inertia tensor's time derivative, DS lengths and DS velocities, unit quaternion components, and time derivative of the unit quaternion components, and $\Theta \in \mathbb{R}^2$ is a vector of uncertain constant parameters, defined as $\Theta \triangleq [\, C_D\rho \quad 1\,]^T$.

The open-loop error system in Eq. (23) can be expressed as

$$\dot{r} = Y\widetilde{\Theta} + Y\widehat{\Theta} + \alpha \dot{e}_v \tag{25}$$

where the parameter estimation error $\widetilde{\Theta} \in \mathbb{R}^2$ is defined as

$$\widetilde{\Theta} \triangleq \Theta - \widehat{\Theta} \tag{26}$$

In Eq. (26), the parameter estimate $\widehat{\Theta} \in \mathbb{R}^2$ is defined as $\widehat{\Theta} \triangleq [\widehat{C_D}\ \hat{\rho}\quad 1]^T$, where $\widehat{C_D}$, $\hat{\rho} \in \mathbb{R}$ are the estimates of C_D and ρ, respectively. To form a closed-loop error system, we define an auxiliary controller $\bar{u} \in \mathbb{R}^3$ as

$$\bar{u} \triangleq Y\widehat{\Theta} \tag{27}$$

Substituting the auxiliary controller Eq. (27) into the open-loop error system Eq. (25) yields

$$\dot{r} = Y\widetilde{\Theta} + \bar{u} + \alpha \dot{e}_v \tag{28}$$

and Eq. (28) can be rewritten as

$$\dot{r} = Y\widetilde{\Theta} + \bar{u}_d + \chi + \alpha \dot{e}_v \tag{29}$$

where the auxiliary signal $\chi \in \mathbb{R}^3$ is defined as

$$\chi \triangleq \bar{u} - \bar{u}_d \tag{30}$$

To facilitate the closed-loop error system, the desired auxiliary controller $\bar{u}_d \in \mathbb{R}^3$ is defined as

$$\bar{u}_d \triangleq -kr - \alpha \dot{e}_v - \beta e_v \tag{31}$$

where $\beta \in \mathbb{R}_{>0}$ is a constant positive control gain, and $k \in \mathbb{R}^{3\times3}_{>0}$ is a constant, positive-definite, diagonal, control gain matrix.

Assumption 1: The auxiliary term χ can be upper bounded by a positive constant, i.e., $\|\chi\| \leq \epsilon$ for $\epsilon \in \mathbb{R}_{>0}$.

Remark 2: To minimize the error between Eqs. (27) and (31), five parameters can be varied, i.e., Y, $\widehat{\Theta}$, k, α, β. By altering the deployment levels of the DSs, values of the atmospheric torque, the gravity gradient torque, and inertia tensor are changed, and the value of Y can be altered. The parameter $\widehat{\Theta}$ is updated according to Eq. (36); therefore, the value of Eq. (27) can be modified. The control gains k, α, β can be selected directly by the user to influence the designed values in Eq. (31). Each of these values can be modified by the user to make the minimization realizable. The minimization can be achieved using numerical methods, e.g., MATLAB's fmincon function. By satisfying the desired control law in Eq. (31), the value of Y can be computed to satisfy the bounding condition described in Assumption 1.

Substituting Eq. (31) into Eq. (29) yields the closed-loop error system

$$\dot{r} = Y\widetilde{\Theta} - kr - \beta e_v + \chi \tag{32}$$

To facilitate the development of the adaptation law, Eq. (23) can be rewritten as

$$\dot{r} - \alpha \dot{e}_v = Y\Theta \tag{33}$$

and the integral of the left-hand side of Eq. (33) can be expressed over an integration window of $\Delta t \in \mathbb{R}_{>0}$ as

$$\mathcal{U}(\Delta t, t) \triangleq \int_{t-\Delta t}^{t} (\dot{r}(\sigma) - \alpha \dot{e}_v(\sigma))\, \mathrm{d}\sigma \tag{34}$$

The integral of the regression matrix Y in Eq. (24) is defined as

$$\mathcal{Y}(\Delta t, t) \triangleq \int_{t-\Delta t}^{t} Y(\sigma)\, \mathrm{d}\sigma \tag{35}$$

The implementable form of the ICL-based adaptation law for the parameter estimates is designed as [20,21]

$$\dot{\widehat{\Theta}} \triangleq \mathrm{proj}\left(\Gamma_{\mathrm{ICL}} Y^T r + \Gamma_{\mathrm{ICL}} k_{\mathrm{ICL}} \sum_{i=1}^{N} \mathcal{Y}_i^T \left(\mathcal{U}_i - \mathcal{Y}_i \widehat{\Theta}\right)\right) \tag{36}$$

where $\mathrm{proj}(\cdot)$ denotes the continuous projection algorithm defined in Appendix E of [28], which is used to guarantee that $\widehat{\Theta}(t)$ stays within the known region of Θ. In Eq. (36), k_{ICL}, $\Gamma_{\mathrm{ICL}} \in \mathbb{R}^{2\times2}_{>0}$ are constant, positive-definite, diagonal, control gain matrices, $N \in \mathbb{Z}_{>0}$ denotes the number of stored input–output data pairs, and $\mathcal{Y}_i \triangleq \mathcal{Y}(t_i)$, $\mathcal{U}_i \triangleq \mathcal{U}(t_i)$, and $t_i \in [0, t]$ are time points between the initial time and the current time. To facilitate the subsequent stability analysis, substituting $\mathcal{U}(\Delta t, t) = \mathcal{Y}\Theta$ and Eq. (26) into Eq. (36) yields the following equivalent analytical form of the adaptation law in Eq. (36) as

$$\dot{\widehat{\Theta}} \triangleq \mathrm{proj}\left(\Gamma_{\mathrm{ICL}} Y^T r + \Gamma_{\mathrm{ICL}} k_{\mathrm{ICL}} \sum_{i=1}^{N} \mathcal{Y}_i^T \mathcal{Y}_i \widetilde{\Theta}\right) \tag{37}$$

Assumption 2: Assuming that the system is sufficiently excited over a finite duration of time (FE condition), then there exists a finite time $\bar{T} \in \mathbb{R}_{>0}$ such that

$$\lambda_{\min}\left\{\sum_{i=1}^{N} \mathcal{Y}_i^T \mathcal{Y}_i\right\} \geq \lambda \tag{38}$$

where $\lambda \in \mathbb{R}_{>0}$ is an arbitrarily small constant, and the threshold value is related to the exponential convergence rate of the system, as shown in the subsequent stability analysis.

V. Stability Analysis

Two theorems are provided in this section. Theorem 1 shows that the tracking errors $r(t)$ and $e_v(t)$ remain bounded for all $t < \overline{T}$, and Theorem 2 concludes that the tracking errors $r(t)$ and $e_v(t)$ converge exponentially to a bounded region and the product of the drag coefficient and atmospheric density are identified when the FE condition is satisfied.

Theorem 1: For the attitude dynamics in Eq. (4), the auxiliary controller in Eq. (31) and adaptive update law in Eq. (36) ensure that the attitude tracking errors $r(t)$ and $e_v(t)$ remain bounded, provided that Assumption 1 and the gain condition $\lambda_{\min}\{k\} > (1/2)$ are satisfied in the sense that

$$\|y(t)\|^2 \leq b_1 \exp(-b_2 t) + b_3 \tag{39}$$

for all $t \in [0, \overline{T})$, where $b_1 \triangleq (B_{\overline{V}}/B_{\underline{V}})\|y(0)\|^2 \in \mathbb{R}_{>0}$, $b_2 \triangleq (\lambda_1/B_{\overline{V}}) \in \mathbb{R}_{>0}$, $b_3 \triangleq (B_{\overline{V}}/(2\lambda_1 B_{\underline{V}}))\epsilon^2 + ((\overline{b} - \underline{b})/B_{\underline{V}}) \in \mathbb{R}_{>0}$, $\lambda_1 \triangleq \min\{\lambda_{\min}\{k\} - (1/2), \beta \cdot \lambda_{\min}\{\alpha\}\} \in \mathbb{R}_{>0}$, $B_{\underline{V}} \triangleq (1/2)\min\{1, \beta\} \in \mathbb{R}_{>0}$, $B_{\overline{V}} \triangleq (1/2)\max\{1, \beta\} \in \mathbb{R}_{>0}$, and $\underline{b}$, $\overline{b} \in \mathbb{R}_{>0}$.

Proof: Let $V \in \mathbb{R}_{\geq 0}$ be a candidate Lyapunov function defined as

$$V \triangleq \frac{1}{2} r^T r + \frac{\beta}{2} e_v^T e_v + \frac{1}{2} \widetilde{\Theta}^T \Gamma_{\mathrm{ICL}}^{-1} \widetilde{\Theta} \tag{40}$$

and a composite error vector $y \in \mathbb{R}^6$ is

$$y \triangleq \begin{bmatrix} r^T & e_v^T \end{bmatrix}^T \tag{41}$$

The candidate Lyapunov function can be bounded as

$$B_{\underline{V}}\|y\|^2 + \underline{b} \leq V(y) \leq B_{\overline{V}}\|y\|^2 + \overline{b} \tag{42}$$

where $B_{\underline{V}}$, $B_{\bar{V}}$, $\underline{b}$, $\overline{b}$ are known positive bounding constants. Substituting Eq. (20) and the closed-loop error system in Eq. (32) into the time derivative of Eq. (40) yields

$$\dot{V} = r^T Y\widetilde{\Theta} - r^T kr + r^T \chi - \beta e_v^T \alpha e_v - \widetilde{\Theta}^T \Gamma_{\mathrm{ICL}}^{-1} \dot{\widehat{\Theta}} \tag{43}$$

Substituting the analytical form of the adaptation law in Eq. (37) into Eq. (43) yields

$$\dot{V} = -r^T k r + r^T \chi - \beta e_v^T \alpha e_v - \widetilde{\Theta}^T k_{\text{ICL}} \sum_{i=1}^{N} \mathcal{Y}_i^T \mathcal{Y}_i \widetilde{\Theta} \tag{44}$$

When $t \in [0, \overline{T})$, using Assumption 1, Eq. (44) can be upper bounded as

$$\dot{V} \leq -\lambda_{\min}\{k\}\|r\|^2 - \beta \cdot \lambda_{\min}\{\alpha\}\|e_v\|^2 + \|r\|\epsilon \tag{45}$$

since $\sum_{i=1}^{N} \mathcal{Y}_i^T \mathcal{Y}_i$ is positive semidefinite. Using Young's inequality, Eq. (45) can be further upper bounded as

$$\dot{V} \leq -\left(\lambda_{\min}\{k\} - \frac{1}{2}\right)\|r\|^2 - \beta \cdot \lambda_{\min}\{\alpha\}\|e_v\|^2 + \frac{1}{2}\epsilon^2 \tag{46}$$

By satisfying the condition $\lambda_{\min}\{k\} > (1/2)$, Eq. (46) can be written as

$$\dot{V} \leq -\lambda_1 \|y\|^2 + \frac{1}{2}\epsilon^2 \tag{47}$$

where λ_1 is defined in Eq. (39). By invoking the Comparison Lemma from [29] and using Eq. (42),

$$V(t) \leq V(0)\exp\left(-\frac{\lambda_1}{B_{\overline{V}}}t\right) + \left(\frac{B_{\overline{V}}}{2\lambda_1}\epsilon^2 + \overline{b}\right)\left(1 - \exp\left(-\frac{\lambda_1}{B_{\overline{V}}}t\right)\right) \tag{48}$$

then substituting Eq. (42) into Eq. (48) yields Eq. (39).

From Eqs. (39) and (41), the tracking errors $r(t)$ and $e_v(t)$ remain bounded for all $t \in [0, \overline{T})$. Using Eq. (14), since $e_v(t) \in \mathcal{L}_\infty$, then $e_0(t) \in \mathcal{L}_\infty$. Using Eq. (20), since $r(t)$, $e_v(t) \in \mathcal{L}_\infty$, then $\dot{e}_v(t) \in \mathcal{L}_\infty$. Since $\dot{e}_v(t), e_v(t), e_0(t) \in \mathcal{L}_\infty$, using Eq. (21) yields $\tilde{\omega}(t) \in \mathcal{L}_\infty$. Since $e_v(t), \tilde{\omega}(t) \in \mathcal{L}_\infty$, using Eq. (22) yields $\dot{e}_0(t) \in \mathcal{L}_\infty$. Since $r(t)$, $\dot{e}_v(t)$, $e_v(t) \in \mathcal{L}_\infty$, using Eq. (31) yields $\bar{u}_d(t) \in \mathcal{L}_\infty$. From Assumption 1, $\chi(t) \in \mathcal{L}_\infty$, then $\bar{u}(t) \in \mathcal{L}_\infty$ using Eq. (30). Using the projection algorithm in Eq. (36), $\widehat{\Theta}(t) \in \mathcal{L}_\infty$. Since $\bar{u}(t)$, $\widehat{\Theta}(t) \in \mathcal{L}_\infty$, $Y(t) \in \mathcal{L}_\infty$ using Eq. (27). Additional bounding arguments can be used to show that all other signals remain bounded. □

Theorem 2: For the attitude dynamics in Eq. (4), the auxiliary controller in Eq. (31) and adaptive update law in Eq. (36) ensure that the attitude tracking error and the parameter estimation errors are uniformly ultimately bounded, provided that Assumptions 1 and 2 and the gain condition $\lambda_{\min}\{k\} > (1/2)$ are satisfied in the sense that

$$\|z(t)\|^2 \leq c_1 \exp(-c_2 t) + c_3 \tag{49}$$

for all $t \in [0, \infty)$, where $c_1 \triangleq (C_{\overline{V}}/C_{\underline{V}})\|z(0)\|^2 \exp[(\lambda_2/C_{\overline{V}})\overline{T}] \in \mathbb{R}_{>0}$, $c_2 \triangleq (\lambda_2/C_{\overline{V}}) \in \mathbb{R}_{>0}$, $c_3 \triangleq [(B_{\overline{V}}/(2\lambda_1 C_{\underline{V}}))\epsilon^2 + (\overline{b}/C_{\underline{V}})] \times \exp[(\lambda_2/C_{\overline{V}})\overline{T}] + (C_{\overline{V}}/(2\lambda_2 C_{\underline{V}}))\epsilon^2 \in \mathbb{R}_{>0}$, $\lambda_2 \triangleq \min\{\lambda_{\min}\{k\} - (1/2), \beta \cdot \lambda_{\min}\{\alpha\}, \lambda \cdot \lambda_{\min}\{k_{\text{ICL}}\}\} \in \mathbb{R}_{>0}$, $C_{\underline{V}} \triangleq (1/2)\min\{1, \beta, \lambda_{\min}\{\Gamma_{\text{ICL}}^{-1}\}\} \in \mathbb{R}_{>0}$, and $C_{\overline{V}} \triangleq (1/2)\max\{1, \beta, \lambda_{\max}\{\Gamma_{\text{ICL}}^{-1}\}\} \in \mathbb{R}_{>0}$.

Proof: Let V be the candidate Lyapunov function defined in Eq. (40), and define another composite error vector $z \in \mathbb{R}^8$ as

$$z \triangleq \begin{bmatrix} r^T & e_v^T & \widetilde{\Theta}^T \end{bmatrix}^T \tag{50}$$

The candidate Lyapunov function in Eq. (40) can be bounded as

$$C_{\underline{V}}\|z\|^2 \leq V(z) \leq C_{\overline{V}}\|z\|^2 \tag{51}$$

where $C_{\underline{V}}$, $C_{\overline{V}} \in \mathbb{R}_{>0}$ are the known bounding constants. From Assumption 2, $\sum_{i=1}^{N} \mathcal{Y}_i^T \mathcal{Y}_i$ is positive definite for $t \geq \overline{T}$, and therefore Eq. (44) can be upper bounded as

$$\dot{V} \leq -\left(\lambda_{\min}\{k\} - \frac{1}{2}\right)\|r\|^2 - \beta \cdot \lambda_{\min}\{\alpha\}\|e_v\|^2 - \lambda \cdot \lambda_{\min}\{k_{\text{ICL}}\}\|\widetilde{\Theta}\|^2 + \frac{1}{2}\epsilon^2 \tag{52}$$

where the gain condition $\lambda_{\min}\{k\} > (1/2)$ must be satisfied. Using Eq. (51), Eq. (52) can be further upper bounded as

$$\dot{V} \leq -\lambda_2\|z\|^2 + \frac{1}{2}\epsilon^2 \tag{53}$$

where λ_2 is defined in Eq. (49). By invoking the Comparison Lemma from [29] and using Eq. (51),

$$V(t) \leq V(\overline{T})\exp\left(-\frac{\lambda_2}{C_{\overline{V}}}(t - \overline{T})\right) + \frac{C_{\overline{V}}}{2\lambda_2}\epsilon^2\left(1 - \exp\left(-\frac{\lambda_2}{C_{\overline{V}}}(t - \overline{T})\right)\right) \tag{54}$$

Using the result in Theorem 1, i.e., Eq. (48), yields

$$V(\overline{T}) \leq V(0) + \frac{B_{\overline{V}}}{2\lambda_1}\epsilon^2 + \overline{b} \tag{55}$$

Substituting Eqs. (50), (51), and (55) into Eq. (54) yields Eq. (49). Using the similar bounding arguments, $e_0(t)$, $\dot{e}_0(t)$, $e_v(t)$, $\dot{e}_v(t)$, $r(t)$, $\tilde{\omega}(t)$, $\bar{u}_d(t)$, $\bar{u}(t)$, $\widetilde{\Theta}(t)$, $\widehat{\Theta}(t)$, $Y(t) \in \mathcal{L}_\infty$. □

VI. Simulation

Two numerical simulations (i.e., the regulation simulation in Sec. VI.A and the tracking simulation in Sec. VI.B) were performed to demonstrate the validity of the designed auxiliary controller and the adaptation law.[§§] Integration of the nonlinear attitude dynamics was performed using the fourth-order Runge–Kutta method in MATLAB. The auxiliary signal $\chi(t)$ was minimized using the MATLAB's *fmincon* function.

The simulation started on January 5th, 2018, at 00:00 UT, and the deployment level of each DS was calculated every 30 s. The spacecraft was simulated in an International Space Station (ISS)–like orbit with 51 deg inclination and 400 km altitude. The initial conditions were selected as shown in Table 1. The variable atmospheric density obtained from the NRLMSISE-00 empirical model [10] is used for propagating the dynamics and used for comparison with the learned uncertain parameter.

Remark 3: The deployment level of each DS was calculated every 30 s. A smaller time step could be used; however, 30 s sampling provided a practical balance between the attitude error transient response and the computational demands. The regulation simulation required an average of 340 s for a 10 h of simulation to complete using a macOS Catalina operating system, 2.9 GHz Dual-Core Intel Core i5 processor, and 8 GB 2133 MHz LPDDR3 memory computer. The tracking simulation takes an average of 379 s for a 10 h of simulation with the same machine specifications to complete.

To achieve the regulation and tracking objectives, the controller gains were selected as

[§§]The regulation objective in Sec. VI.A indicates that the configuration of the spacecraft is regulated to the desired constant attitude angles with respect to the orbit frame, and the tracking objective in Sec. VI.B indicates that the configuration of the spacecraft is tracking the desired time-varying roll angle with respect to the orbit frame.

Table 1 Initial conditions of the orbit for the spacecraft

Semimajor axis	Eccentricity	True anomaly	RAAN	Argument of perigee	Orbit inclination
6778×10^3 km	0	108.08 deg	206.36 deg	101.07 deg	51 deg

RAAN = Right ascension of the ascending node.

Table 2 Physical characteristics of the spacecraft

Mass of the body	Mass of the boom	Maximum boom length	Boom width	Nominal value of C_D
3.0 kg	9.0×10^{-2} kg	3.7 m	3.8×10^{-2} m	2.2

$$\alpha = 10^{-2} \times \begin{bmatrix} 0.3 & 0 & 0 \\ 0 & 1.0 & 0 \\ 0 & 0 & 2.2 \end{bmatrix}, \qquad \beta = 5.0 \times 10^{-7},$$

$$k = 10^{-2} \begin{bmatrix} 0.2 & 0 & 0 \\ 0 & 0.3 & 0 \\ 0 & 0 & 1.2 \end{bmatrix}, \qquad k_{\mathrm{ICL}} = 10^{-3} \begin{bmatrix} 5.0 & 0 \\ 0 & 1.0 \end{bmatrix},$$

$$\Gamma_{\mathrm{ICL}} = 10^{-17} \begin{bmatrix} 1.0 & 0 \\ 0 & 1.0 \end{bmatrix}$$

The physical parameters of the spacecraft used in the simulation are shown in Table 2.

Remark 4: For visualization purpose, a 3-2-1 Euler angles rotation sequence, which brings the orbital frame to the body coordinate system, is used to represent the spacecraft orientation. Specifically, $\phi, \theta, \psi \in \mathbb{R}$ represent the roll, pitch, and yaw angle of the spacecraft, respectively, $\dot{\phi}, \dot{\theta}, \dot{\psi} \in \mathbb{R}$ represent their time derivatives, and $\phi_d, \theta_d, \psi_d \in \mathbb{R}$ represent the desired orientation. The unit quaternion $q(q_0, q_v)$ used by the controller is transformed into attitude angles (i.e., ϕ, θ, ψ) using the MATLAB aerospace toolbox.

A. Regulation

The initial conditions and desired orientation of the spacecraft (in Euler angles) were selected as indicated in Table 3. Figure 2 shows the tracking of the desired spacecraft orientation in quaternion representation for the regulation control objective, and Fig. 3 shows the quaternion error signals, which satisfies the conditions given in Eq. (18) for attitude tracking/regulation. As shown in Fig. 4, when the system reaches steady state, the roll, pitch, and yaw angles are regulated to the desired roll, pitch, and yaw angles, with steady-state errors of $\pm 4.0 \times 10^{-2}$ deg, $\pm 8.6 \times 10^{-4}$ deg, and $\pm 9.1 \times 10^{-3}$ deg, respectively. Figure 5 shows the boom lengths throughout the simulation. For the given initial conditions, the DSs are required to extend/retract at a rate of change that could induce disturbances to the spacecraft and with a desired amplitude that is larger than the available DS length (i.e., actuator saturation). However, the robustness of the controller demonstrates that despite the unmodeled saturation limits, the controller is able to achieve the control objective. Figure 6 shows the mismatch between the actual and desired auxiliary control inputs expressed in Eqs. (27) and (31). When the system reaches steady state, the norm of the torque difference is regulated within 3.0×10^{-8} N · m.

As described in Eq. (2), the theoretical development is based on the typical assumption that the atmospheric density is an uncertain constant [1,5]. However, the more realistic NRLMSISE-00 model is used in the simulation to illustrate the robustness of the developed controller/estimator. The NRLMSISE-00 model includes time-varying perturbations about a mean value (i.e., the typically assumed constant atmospheric density). Despite the unmodeled time-varying perturba-

Table 3 Initial conditions for the regulation objective

$\phi_0 = 80$ deg	$\theta_0 = -60$ deg	$\psi_0 = 50$ deg
$\dot{\phi}_0 = 0.02$ deg/s	$\dot{\theta}_0 = -0.03$ deg/s	$\dot{\psi}_0 = 0.025$ deg/s
$\phi_d = 45$ deg	$\theta_d = 0$ deg	$\psi_d = 0$ deg

$$\hat{\Theta}_0 = [\,1.4 \times 10^{-11} \quad 1\,]^T \ \mathrm{kg/m^3}$$

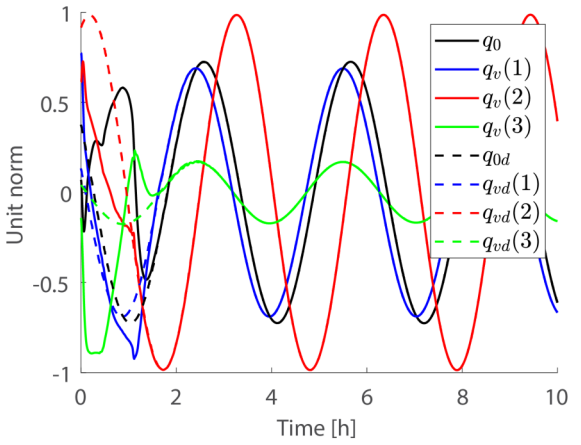

Fig. 2 Spacecraft configuration tracking (quaternion) for the regulation objective.

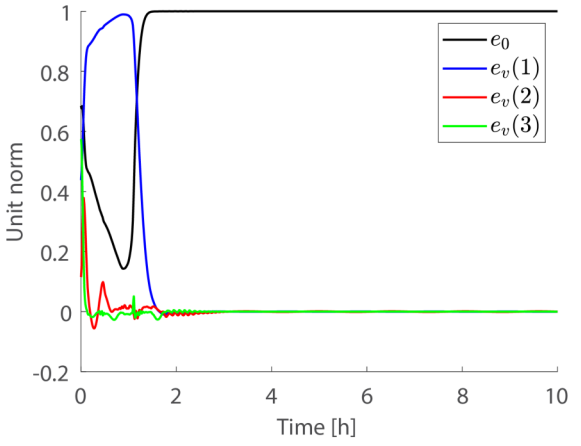

Fig. 3 Spacecraft configuration error for the regulation objective.

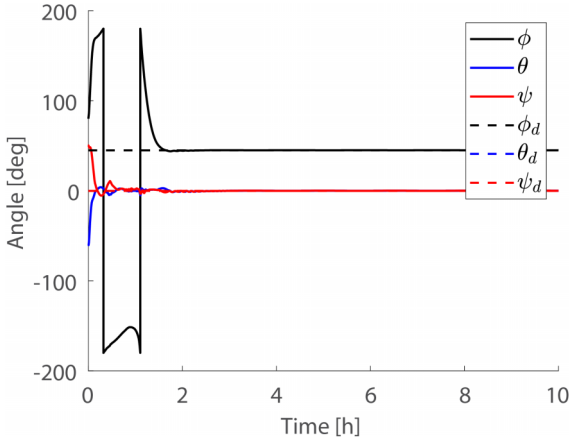

Fig. 4 Configuration regulation with real-time roll ϕ, pitch θ, and yaw ψ vs the desired roll ϕ_d, pitch θ_d, and yaw ψ_d attitude angles, respectively.

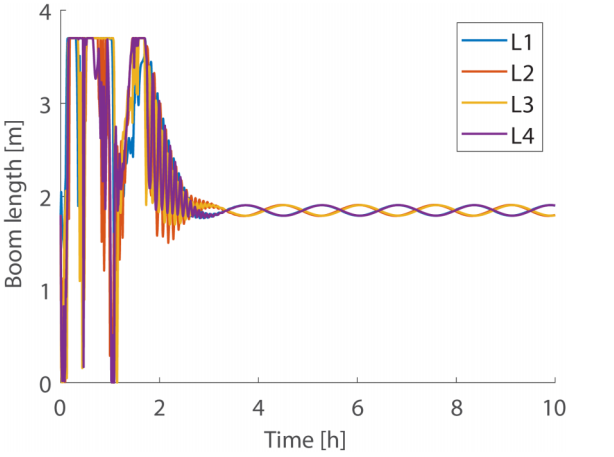

Fig. 5 Boom lengths of the CubeSat drag maneuvering device in real-time for the regulation objective.

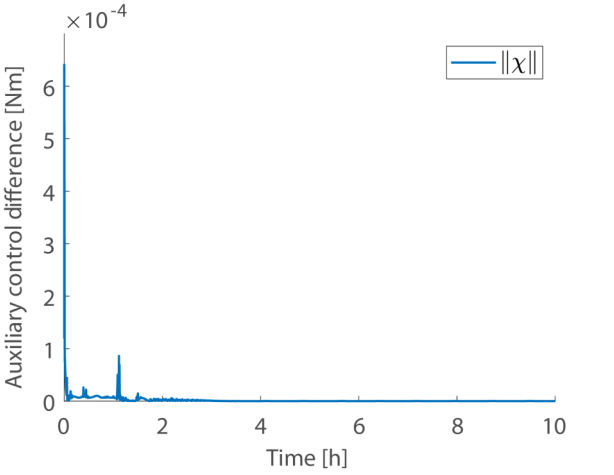

Fig. 6 Auxiliary control difference for the regulation objective.

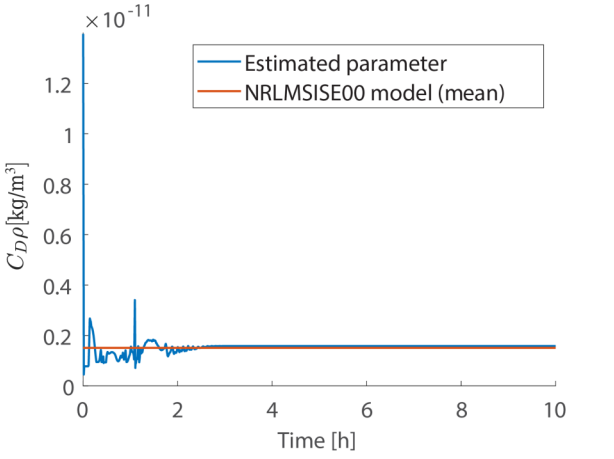

Fig. 7 Estimated parameter value and true parameter value for the regulation objective.

tions, Fig. 7 indicates that the ICL adaptation method is able to approximate the product of the drag coefficient with the mean atmospheric density with approximately 4.8% steady-state error (i.e., 1.509×10^{-12} kg/m^3 true vs 1.582×10^{-12} kg/m^3 estimated). Figure 8 shows the root-mean-square (RMS) error between the estimated parameter value and the true parameter value, and the RMS error is significantly decreasing to a small level when compared with the magnitude of the real density.

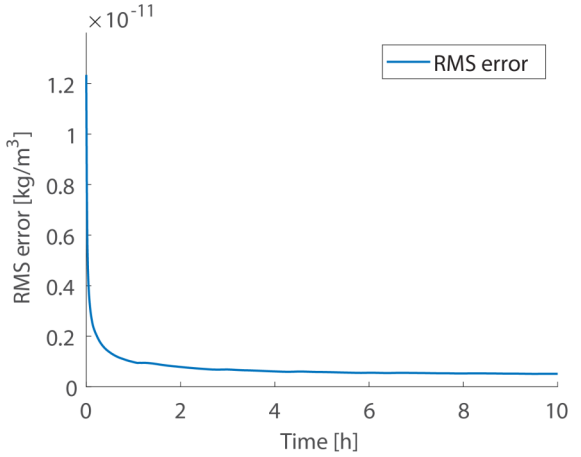

Fig. 8 Root-mean-square error between the estimated parameter value and true parameter value for the regulation objective.

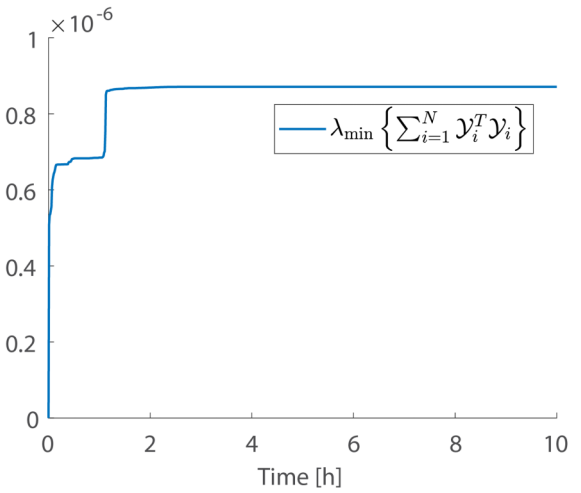

Fig. 9 The minimum eigenvalue of the history stack, i.e., $\lambda_{\min}\{\sum_{i=1}^{N} \mathcal{Y}_i^T \mathcal{Y}_i\}$, for the regulation objective.

To incorporate the ICL term in the adaptation law, the history stack (i.e., $\sum_{i=1}^{N} \mathcal{Y}_i^T \mathcal{Y}_i$) is appended to the adaptation law at each time step as shown in Eq. (38). To improve the parameter estimation performance, the minimum eigenvalue of the history stack (i.e., $\lambda_{\min}\{\sum_{i=1}^{N} \mathcal{Y}_i^T \mathcal{Y}_i\}$) is evaluated at each time step and compared with the minimum eigenvalue of the history stack at the previous time step. The value of λ is updated only when the current value is larger than the previous value because larger λ indicates faster parameter convergence according to Eq. (49) [30]. Figure 9 shows the minimum eigenvalue of the history stack, i.e., $\lambda_{\min}\{\sum_{i=1}^{N} \mathcal{Y}_i^T \mathcal{Y}_i\}$.

B. Tracking

To achieve the tracking objective, the desired orientation of the spacecraft with respect to the orbital frame was changed to a time-varying function. In addition to validate the robustness of the designed controller, values of the initial conditions for the attitude angle rates (i.e., $\dot{\phi}_0, \dot{\theta}_0$, and $\dot{\psi}_0$) were increased. The initial conditions

Table 4 Initial conditions for the tracking objective

$\phi_0 = 80$ deg	$\theta_0 = -60$ deg	$\psi_0 = 50$ deg
$\dot{\phi}_0 = 0.5$ deg/s	$\dot{\theta}_0 = -1$ deg/s	$\dot{\psi}_0 = 1$ deg/s
$\phi_d = \sin[(\pi/6000)t]$ deg	$\theta_d = 0$ deg	$\psi_d = 0$ deg
$\hat{\Theta}_0 = [1.4 \times 10^{-11} \quad 1]^T$ kg/m^3		

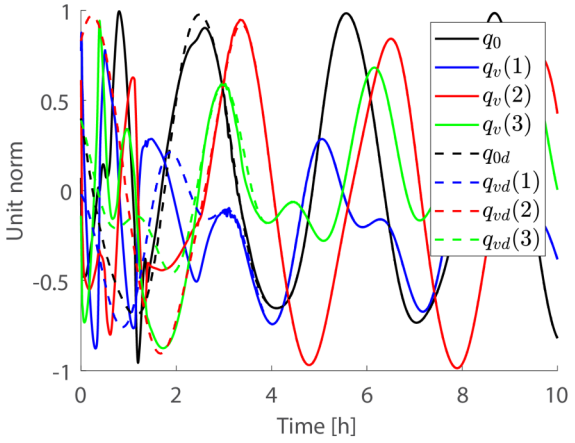

Fig. 10 Spacecraft configuration tracking (quaternion) for the tracking objective.

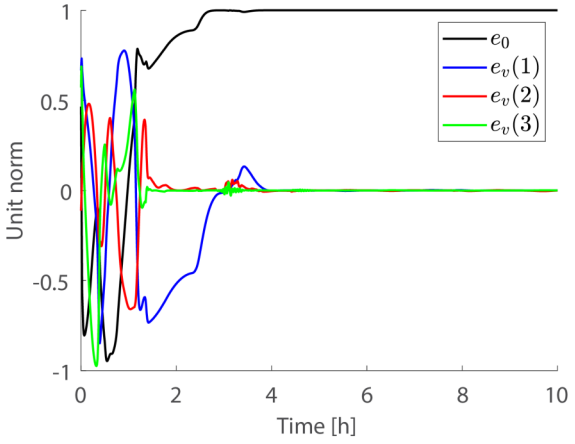

Fig. 11 Spacecraft configuration error for the tracking objective.

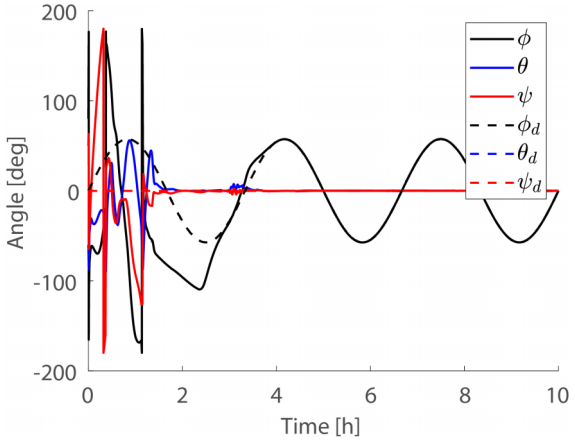

Fig. 12 Configuration tracking with real-time roll ϕ, pitch θ, and yaw ψ vs the desired roll ϕ_d, pitch θ_d, and yaw ψ_d attitude angles, respectively.

and desired orientation of the spacecraft for the tracking objective were selected as indicated in Table 4.¶¶

Similar to the regulation objective, Fig. 10 shows the tracking of the desired spacecraft orientation in quaternion representation for the tracking objective. Figure 11 shows the quaternion error signals, and the control objective is also achieved as the result in Fig. 11 is matching with Eq. (18). As shown in Fig. 12, the orientation of the

¶¶The unit for time is second.

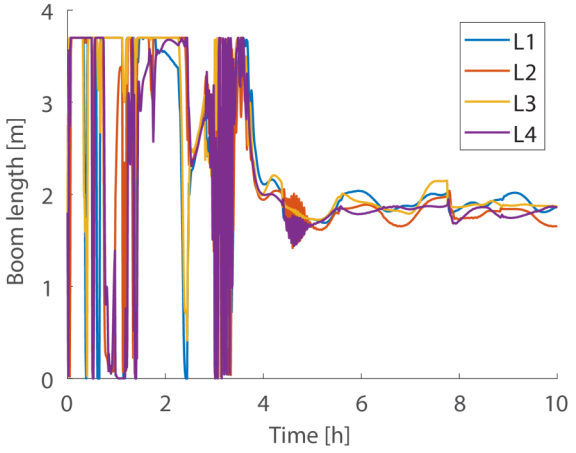

Fig. 13 Boom lengths of the CubeSat drag maneuvering device in real-time for the tracking objective.

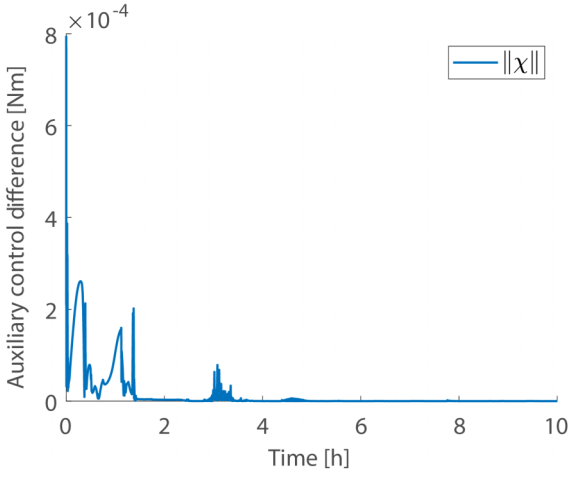

Fig. 14 Auxiliary control difference for the tracking objective.

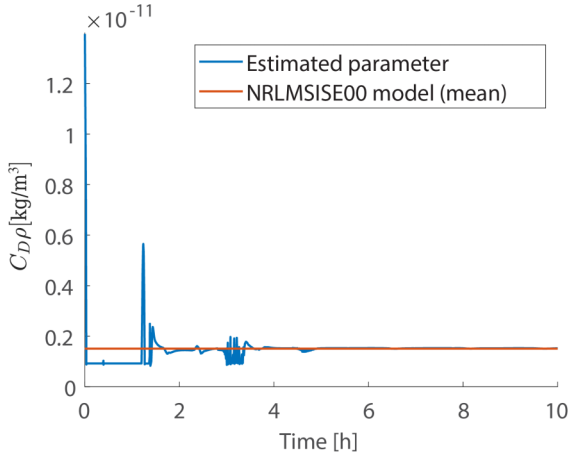

Fig. 15 Estimated parameter value and true parameter value for the tracking objective.

spacecraft is tracking the desired time-varying orientation for the roll angle*** (i.e., $\phi_d = \sin[(\pi/6000)t]$ deg). When the system reaches steady state, the roll, pitch, and yaw angles are tracking the desired roll, pitch, and yaw angles, with steady-state errors of $\pm 1.0 \times 10^{-2}$ deg,

***A typical example for a given desired roll trajectory tracking is Earth observation mission. Specifically, the spacecraft can observe Earth from the orbit at different viewing angles.

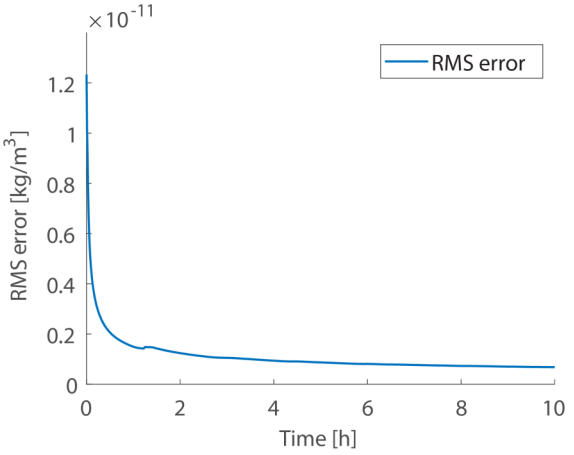

Fig. 16 Root-mean-square error between the estimated parameter value and true parameter value for the tracking objective.

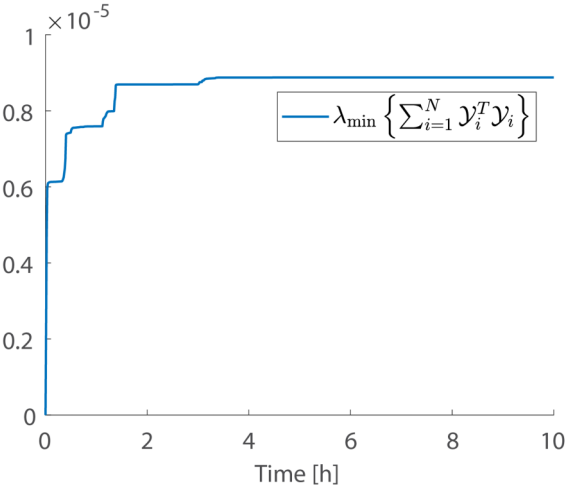

Fig. 17 The minimum eigenvalue of the history stack, i.e., $\lambda_{\min}\{\sum_{i=1}^{N} \mathcal{Y}_i^T \mathcal{Y}_i\}$, for the tracking objective.

$\pm 6.0 \times 10^{-2}$ deg, and $\pm 8.0 \times 10^{-2}$ deg, respectively. Figure 13 shows the boom lengths throughout the simulation for the tracking objective. Figure 14 shows the mismatch between the actual and desired auxiliary control inputs expressed in Eqs. (27) and (31) for the tracking objective. When the system reaches steady state, the norm of the torque difference is regulated within 4.2×10^{-8} N · m. Figure 15 indicates the estimated parameter value and the true parameter value comparison for the tracking objective. The steady-state error is approximately 0.93% (i.e., 1.509×10^{-12} kg/m^3 true vs 1.523×10^{-12} kg/m^3 estimated). Figure 16 shows the RMS error between the estimated parameter value and the true parameter value for the tracking objective. Figure 17 shows the minimum eigenvalue of the history stack, i.e., $\lambda_{\min}\{\sum_{i=1}^{N} \mathcal{Y}_i^T \mathcal{Y}_i\}$ for the tracking objective.

VII. Conclusions

An adaptive control method is presented to track the desired attitude trajectory of a CubeSat using a DMD regardless of the uncertain drag coefficient and atmospheric density parameters. By using retractable DSs, the atmospheric and gravity gradient torques are exploited to track a given attitude trajectory. A time derivative of the inertia tensor term is included in the dynamics, and the control inputs are isolated on one side of the equation. An optimization is used to minimize the difference between the value of actual auxiliary control inputs and the value of designed auxiliary control inputs. An ICL approach is implemented to compensate for the uncertain parameter. Two simulation examples are performed to illustrate the proposed controller and adaptation law design.

Acknowledgments

This research is supported in part by the Air Force Office of Scientific Research award number FA9550-19-1-0169 and the Fulbright Colombia Commission. Any opinions, findings, and conclusions or recommendations expressed in this material are those of the authors and do not necessarily reflect the views of the sponsoring agency.

References

[1] Bevilacqua, R., and Romano, M., "Rendezvous Maneuvers of Multiple Spacecraft Using Differential Drag Under J2 Perturbation," *Journal of Guidance, Control, and Dynamics*, Vol. 31, No. 6, 2008, pp. 1595–1607. https://doi.org/10.2514/1.36362

[2] Guglielmo, D., Omar, S., Bevilacqua, R., Fineberg, L., Treptow, J., Poffenberger, B., and Johnson, Y., "Drag Deorbit Device: A New Standard Reentry Actuator for CubeSats," *Journal of Spacecraft and Rockets*, Vol. 56, No. 1, 2019, pp. 129–145. https://doi.org/10.2514/1.A34218

[3] Omar, S. R., and Bevilacqua, R., "Spacecraft Collision Avoidance Using Aerodynamic Drag," *Journal of Guidance, Control, and Dynamics*, Vol. 43, No. 3, 2020, pp. 567–573. https://doi.org/10.2514/1.G004518

[4] Omar, S. R., and Bevilacqua, R., "Hardware and GNC Solutions for Controlled Spacecraft Re-Entry Using Aerodynamic Drag," *Acta Astronautica*, Vol. 159, June 2019, pp. 49–64. https://doi.org/10.1016/j.actaastro.2019.03.051

[5] Sutherland, R., Kolmanovsky, I., and Girard, A. R., "Attitude Control of a 2U Cubesat by Magnetic and Air Drag Torques," *IEEE Transactions on Control Systems Technology*, Vol. 27, No. 3, 2018, pp. 1047–1059. https://doi.org/10.1109/TCST.2018.2791979

[6] Pastorelli, M., Bevilacqua, R., and Pastorelli, S., "Differential-Drag-Based Roto-Translational Control for Propellant-Less Spacecraft," *Acta Astronautica*, Vol. 114, Sept. 2015, pp. 6–21. https://doi.org/10.1016/j.actaastro.2015.04.014

[7] Sun, R., Wang, J., Zhang, D., Jia, Q., and Shao, X., "Roto-Translational Spacecraft Formation Control Using Aerodynamic Forces," *Journal of Guidance, Control, and Dynamics*, Vol. 40, No. 10, 2017, pp. 2556–2568. https://doi.org/10.2514/1.G003130

[8] Guglielmo, D., Omar, S. R., and Bevilacqua, R., "Drag De-Orbit Device (D3): A Retractable Device for CubeSat Attitude and Orbit Control Using Aerodynamic Forces," NASA Technical Reports Server, KSC-E-DAA-TN37922, 2017, https://ntrs.nasa.gov/citations/20170000261.

[9] National Oceanic and Atmospheric Administration, NASA, U.S. Air Force, U.S. Standard Atmosphere, Rept. NOAA-S/T-76-1562, NASA-TM-X-74335, Washington, D.C., 1976, https://ntrs.nasa.gov/citations/19770009539.

[10] Picone, J., Hedin, A., Drob, D. P., and Aikin, A., "NRLMSISE-00 Empirical Model of the Atmosphere: Statistical Comparisons and Scientific Issues," *Journal of Geophysical Research: Space Physics*, Vol. 107, No. A12, 2002, pp. SIA–15. https://doi.org/10.1029/2002 JA009430

[11] Wang, Y., and Xu, S., "Attitude Stability of a Spacecraft on a Stationary Orbit Around an Asteroid Subjected to Gravity Gradient Torque," *Celestial Mechanics and Dynamical Astronomy*, Vol. 115, No. 4, 2013, pp. 333–352. https://doi.org/10.1007/s10569-012-9463-6

[12] Mammarella, M., Lee, D. Y., Park, H., Capello, E., Dentis, M., and Guglieri, G., "Attitude Control of a Small Spacecraft via Tube-Based Model Predictive Control," *Journal of Spacecraft and Rockets*, Vol. 56, No. 6, 2019, pp. 1662–1679. https://doi.org/10.2514/1.A34394

[13] Omar, S., Riano-Rios, C., and Bevilacqua, R., "Semi-Passive Three Axis Attitude Stabilization for Earth Observation Satellites Using the Drag Maneuvering Device," *12th International Academy of Astronautics Symposium on Small Satellites for Earth Observation*, Paper IAA-B12-0701, Berlin, Germany, 2019.

[14] Riano-Rios, C., Omar, S., Bevilacqua, R., and Dixon, W., "Spacecraft Attitude Regulation in Low Earth Orbit Using Natural Torques," *2019 IEEE 4th Colombian Conference on Automatic Control (CCAC)*, Inst. of Electrical and Electronics Engineers, New York, 2019, pp. 1–6. https://doi.org/10.1109/CCAC.2019.8921399

[15] Ioannou, P. A., and Sun, J., *Robust Adaptive Control*, PTR Prentice-Hall, Upper Saddle River, NJ, 1996, Vol. 1, Chaps. 4, 5.

[16] Narendra, K. S., and Annaswamy, A. M., *Stable Adaptive Systems*, Prentice-Hall, Upper Saddle River, NJ, 1989, Chap. 6.

[17] Sastry, S., and Bodson, M., *Adaptive Control: Stability, Convergence and Robustness*, Prentice-Hall, Upper Saddle River, NJ, 1989, Chap. 6.

[18] Chowdhary, G. V., and Johnson, E. N., "Theory and Flight-Test Validation of a Concurrent-Learning Adaptive Controller," *Journal of Guidance, Control, and Dynamics*, Vol. 34, No. 2, 2011, pp. 592–607. https://doi.org/10.2514/1.46866

[19] Chowdhary, G., Yucelen, T., Mühlegg, M., and Johnson, E. N., "Concurrent Learning Adaptive Control of Linear Systems with Exponentially Convergent Bounds," *International Journal of Adaptive Control and Signal Processing*, Vol. 27, No. 4, 2013, pp. 280–301. https://doi.org/10.1002/acs.2297

[20] Parikh, A., Kamalapurkar, R., and Dixon, W. E., "Integral Concurrent Learning: Adaptive Control with Parameter Convergence Using Finite Excitation," *International Journal of Adaptive Control and Signal Processing*, Vol. 33, No. 12, 2019, pp. 1775–1787. https://doi.org/10.1002/acs.2945

[21] Bell, Z. I., Nezvadovitz, J., Parikh, A., Schwartz, E. M., and Dixon, W. E., "Global Exponential Tracking Control for an Autonomous Surface Vessel: An Integral Concurrent Learning Approach," *IEEE Journal of Oceanic Engineering*, Vol. 45, No. 2, 2018, pp. 362–370. https://doi.org/10.1109/JOE.2018.2880622

[22] Riano-Rios, C., Bevilacqua, R., and Dixon, W. E., "Differential Drag-Based Multiple Spacecraft Maneuvering and On-Line Parameter Estimation Using Integral Concurrent Learning," *Acta Astronautica*, Vol. 174, Sept. 2020, pp. 189–203. https://doi.org/10.1016/j.actaastro.2020.04.059

[23] Blackburn, E. P., DeBra, D., Dobrotin, B., Scull, J., Fischell, R. E., Fosth, D., Kelly, J., Fleig, A. J., Perkel, H., Roberson, R. E., Rodden, J., Tinling, B., O'Neil, S., Carroll, F. J., and Bohling, R. F., "NASA Space Vehicle Design Criteria Monograph (Guidance and Control)," NASA SP-8018, March 1969.

[24] Wertz, J. R., Everett, D. F., and Puschell, J. J., *Space Mission Engineering: The New SMAD*, Microcosm Press, Torrance, CA, 2011, pp. 565–600.

[25] Kuipers, J. B., *Quaternions and Rotation Sequences: A Primer with Applications to Orbits, Aerospace, and Virtual Reality*, Princeton Univ. Press, Princeton, NJ, 1999, Chaps. 5, 6.

[26] Costic, B., Dawson, D., De Queiroz, M., and Kapila, V., "Quaternion-Based Adaptive Attitude Tracking Controller Without Velocity Measurements," *Journal of Guidance, Control, and Dynamics*, Vol. 24, No. 6, 2001, pp. 1214–1222. https://doi.org/10.2514/2.4837

[27] MacKunis, W., Dupree, K., Fitz-Coy, N., and Dixon, W., "Adaptive Satellite Attitude Control in the Presence of Inertia and CMG Gimbal Friction Uncertainties," *Journal of the Astronautical Sciences*, Vol. 56, No. 1, 2008, pp. 121–134. https://doi.org/10.1007/BF03256544.

[28] Krstic, M., Kokotovic, P. V., and Kanellakopoulos, I., *Nonlinear and Adaptive Control Design*, Wiley, New York, 1995, pp. 511–514.

[29] Khalil, H. K., *Nonlinear Systems*, 3rd ed., Prentice-Hall, Upper Saddle River, NJ, 2002, Vol. 3, Chaps. 3, 4.

[30] Kamalapurkar, R., Reish, B., Chowdhary, G., and Dixon, W. E., "Concurrent Learning for Parameter Estimation Using Dynamic State-Derivative Estimators," *IEEE Transactions on Automatic Control*, Vol. 62, No. 7, 2017, pp. 3594–3601. https://doi.org/10.1109/TAC.2017.2671343